Fluorescent Silver-AIE Visualization of Neurons and Fibres in the Cleared Brain

Sheng Xie[1, 2, 3#], Alex Y. H. Wong[1#], Kam Chuen[1], Ola Hermanson[4], Nancy Ip[5]*, Ben Zhong Tang[2,6]*, and Sijie Chen[1]*

[1]Ming-Wai Lau Centre for Reparative Medicine, Karolinska Institutet, Hong Kong, China.

[2]Department of Chemistry, Hong Kong Branch of Chinese National Engineering Research Center for Tissue Restoration and Reconstruction, Institute for Advanced Study and HKUST-Shenzhen Research Institute, SCUT-HKUST Joint Research Institute, The Hong Kong University of Science & Technology, Hong Kong, China.

[3]State Key Laboratory of Chemo/Biosensing and Chemometrics, College of Chemistry and Chemical Engineering, Hunan University, Changsha 410082, China.

[4]Department of Neuroscience, Karolinska Institutet, Stockholm, Sweden.

[5]State Key Laboratory of Neuroscience, Division of Biomedical Engineering, and Division of Life Science, The Hong Kong University of Science and Technology, Kowloon, Hong Kong, China.

[6]Shenzhen Institute of Molecular Aggregate Science and Engineering, School of Science and Engineering, The Chinese University of Hong Kong (Shenzhen), Shenzhen 518172, China.

*Corresponding Emails: boip@ust.hk, tangbenz@cuhk.edu.cn, sijie.chen@ki.se

[#]These authors contributed equally.

Abstract

Brain-mapping projects for reconstructing structures and networks in three-dimensions (3D) demand cost-effective, robust, and histologically homogeneous chemical stains for the applications of high-throughput staining in large tissues. Current staining methods such as immunohistology are practically unsustainable for large-scale specimens due to their limited dye-permeability which leads to inhomogeneous performance in thick samples. Herein, we report a novel fluorogenic visualization method for mouse brain tissues by making use of a Ag^+-specific aggregation-induced emission (AIE) strategy after silver impregnation. This novel fluorogenic silver-AIE method surpasses the chromogenic detection used by many conventional silver staining protocols, which have historically made revolutionary contributions to neuroanatomy. This fluorescent silver-based stain allows for analysis of images acquired using wide-field, confocal, SIMs, or light-sheet fluorescence microscopy. We validated the sensitivity, specificity, and versatility of the silver-AIE stain as compared to conventional silver stains and other neuron-specific ones. The fluorogenic AIE method eliminates the high background, artefacts, and poor reproducibility often associated with the reduction of silver solutions. The silver-AIE stain is demonstrated to be highly compatible with immunofluorescence co-staining in paraffin sections and can be applied to hydrogel-based cleared tissue by the passive CLARITY method for image analysis of large tissue slices of 300 μm thick in this study. From this fluorogenic strategy, it is possible for vast types of classic silver staining methods to be modified and re-vitalized.

Introduction

The human brain is composed of billions of interconnected neurons with complex structures and diverse functions. To understand the human brain, researchers worldwide first launched large-scale human brain projects in 2013. Tremendous efforts have been devoted to modern 3D imaging techniques and state-of-the-art technology for the study of neuroanatomy, mesoscale connectome[1], gene expression[2], intact-tissue sequencing of single-cell transcriptome[3], etc., in the nervous system[4,5]. The goal of connectomics is to reconstruct the entirety of the neuronal connections in the whole brain which is essential for the understanding of the brain in fundamental and clinical neuroscience. Classic analysis of the neuronal connectome relies on electron microscopy which requires slow serial sectioning and is computationally intensive for digital reconstruction[6,7]. In other aspects, changes in neuronal morphology are central to brain development and neuroplasticity. This is also associated with numerous neurological disorders[8]. In this regard, the

study of neurodegenerative diseases often require a comprehensive analysis of brain slices at the cellular scale in 3D. Hence, efficient staining methods are required to label neuronal structures specifically and uniformly over a relatively large area of the brain[9].

In the histological staining of neural tissues, silver stains are conventional and yet standard techniques. The very first silver staining method developed by Camillo Golgi in the 1870s[16] and the subsequent Cajal's stain developed by Santiago Ramón y Cajal exploits the special bio-affinity of silver ions towards neural structures and the reduction-based chromogenic silvering reaction. The Cajal's method stains developing neurons in embryos, and moreover gives hyperfine structures of neuron fibers under light microscopy. Interestingly, approximately only 1–5% of neurons in a specimen can be labeled by the Golgi stain for reasons unknown, however this small subset of stained cells offered great detail of neuron morphology due to the sparsity of the stain, making it ideal for observation under light microscopy[17]. In the typical Cajal's stain, the chromogenic visualization is achieved by reducing the silver ions into metallic silver grains, which collectively stains the sample in brown or black. Since the reductive crystallization process depends on microenvironment and has no clear endpoints, the resulting silver grains have a broad range of particle sizes from several nanometers to hundreds of micrometers, leading to varied colors and non-linearity in the chromogenic detection.

The current histological labelling methods for visualization of neural networks include histological stains[12], immunohistochemistry, genetically encoded tags by transgene expression[13], *in situ* hybridization (ISH), and lipophilic tracers for anterograde labelling in connectivity experiments[14,15]. In particular, immunostaining and genetically encoded fluorescent proteins are widely used in brain imaging nowadays which allow selective and fast imaging at multiple scales from molecules to cells with spatiotemporal resolutions[10,11]. Nonetheless, the cost of immunofluorescence staining is usually high and thus unsustainable for staining specimens at large scales. Poor-quality antibodies also lead to non-specific labeling with high background levels. While for expressing fluorescent proteins using transgenic technology, the existing transgenic lines are limited and these fluorescence signals are easily quenched by chemical fixation or paraffin embedding in the preparation of brain slices. An optimized method that allows homogeneous fluorescence labeling of brain blocks in large scale is therefore a key for successful brain-mapping projects.

In search for new fluorescent materials for bioprobes, an atypical photophysical phenomenon known as aggregation-induced emission (AIE) is discovered with promising applications in biology. Unlike conventional luminophores, an AIE luminogen (AIEgen) such as tetraphenylethylene (TPE) has a flexible non-planar structure and emits faintly when molecularly dispersed. In the aggregated state, the AIEgen strongly emit fluorescence due to restriction of molecular motions (RIMs) on account of the physical constraints from neighboring molecules. The fluorescence in responses to molecular states has been explored as a general way to design fluorescent probes for metal ions, small molecules, and biological enzymes[24–27]. Particularly upon binding of the AIE probes to the target, the AIE-based fluorogenic turn-on nature often confers ultrabright labelling, a high signal-to-noise ratio (SNR), and wash-free advantages, thus providing an ideal histological method for tissue imaging analysis.

We have recently proposed a fluorogenic silver-AIE staining method and utilized AIEgen **TPE-4TA** to visualize proteins in the silver-impregnated polyacrylamide gel.[28,29] Taking the advantages of Ag^+ binding by tetrazole-functionalized **TPE-4TA** accompanied with fluorescence emission by the AIE properties, here we explore the strategy of fluorogenic AIE-based silver staining in brain slices in addressing the lack of an efficient and reliable staining method in large-scale brain analysis. A staining protocol modified from the classic silver staining methods (especially the Bielschowsky and Cajal's stain) is established and silver-impregnated brain tissues are analyzed by using advanced fluorescence microscopy.

Results

Design principle and characterization of TPE-4TA as a fluorescent Ag+ probe

The working principle of silver stain utilize the argyrophilic property of nerve cells followed by reduction of Ag^+ to metallic Ag for chromogenic detection. Instead of reducing Ag^+, here we propose to sense Ag^+ in histological sections for fluorogenic detection (Fig. 1). It has been known for a long time that tetrazole compounds can 'precipitate' out silver ions from solutions specifically. In this regards, the anionic tetrazolate moiety in **TPE-4TA** acts as the Ag^+-specific coordination group to trigger the aggregating precipitation, while the AIE-active TPE core endows the responsiveness of aggregation-induced fluorescence emission (Fig. 2a). The resulting

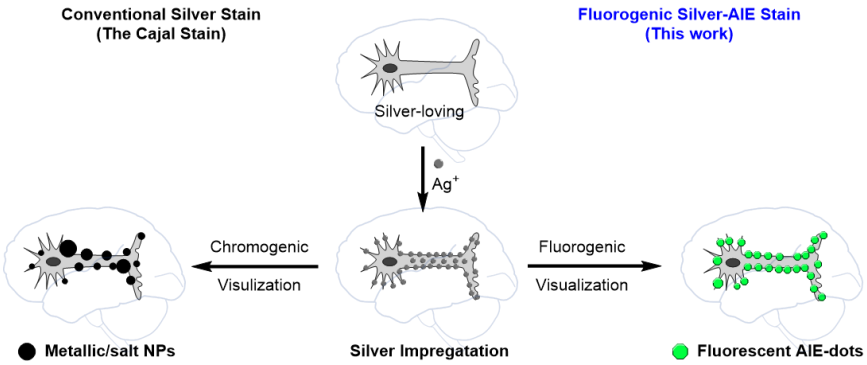

Figure 1. Schematic illustration of the conventional silver stain (the Cajal stain) and the fluorescent silver-AIE stain in this work.

tetrazole-silver complexes are infinite metal-coordination polymers, with anionic tetrazole ring binding to Ag^+ in mono-, bi-, or tri-dentate fashions through coordination and charge–charge interactions (Fig. 2b)[30,31]. These complexes are sparingly soluble in many solvents[32]. A comparison study showed that the aqueous-solubility of tetrazolate-Ag^+ complexes is close to that of Ag_2S (5.5×10^{-51} mol^3/L^3) but is much lower than that of AgCl (1.7×10^{-10} mol^2/L^2). Upon addition of 10 μL of 1 mM **TPE-4TA** into 2 mL of 10 μM silver solution with sonication, stable colloid solutions of silver-tetrazolate AIE-dots were formed with a particle diameter of ~50 ± 15 nm (polydispersity index PDI = 0.32 nm) and a surface-charge of -15 mV as measured by dynamic light scattering (DLS) (Fig. 2c). The negative surface-charge is primarily attributed to the anionic tetrazolate groups on the outer-layer of these nanoparticles. After evaporation of the colloid solution, characterization of the residues by transmission electron microscopy showed nano-sized aggregates with a diameter of ~20 nm, albeit these infinite coordination polymers started to fuse into large particles (Fig. 2c inset).

Due to the unique AIE property, the molecularly dissolved **TPE-4TA** was faintly fluorescent with a photoluminescence quantum yield (PLQY) of ~0.4% due to the free intramolecular motions of the four phenyl rings in the TPE core to dissipate the excited energy. On the other hand, the nanoaggregates of **TPE-4TA** formed were highly fluorescent with a PLQY of ~30%. Fluorescence lifetime measurement also showed a $t_{1/2}$ of ~8 ns for these TPE-4TA nanodots and 1 ns for the dissolved TPE-4TA in solutions (Fig. 2d). As a result, the precipitation process triggered by Ag^+ was instant and vigorous with a spontaneous high-contrast fluorescence turn-on (> 600-fold enhancement) at the peak wavelength of 504 nm (Fig. 2e. These Ag^+-binding and AIE properties

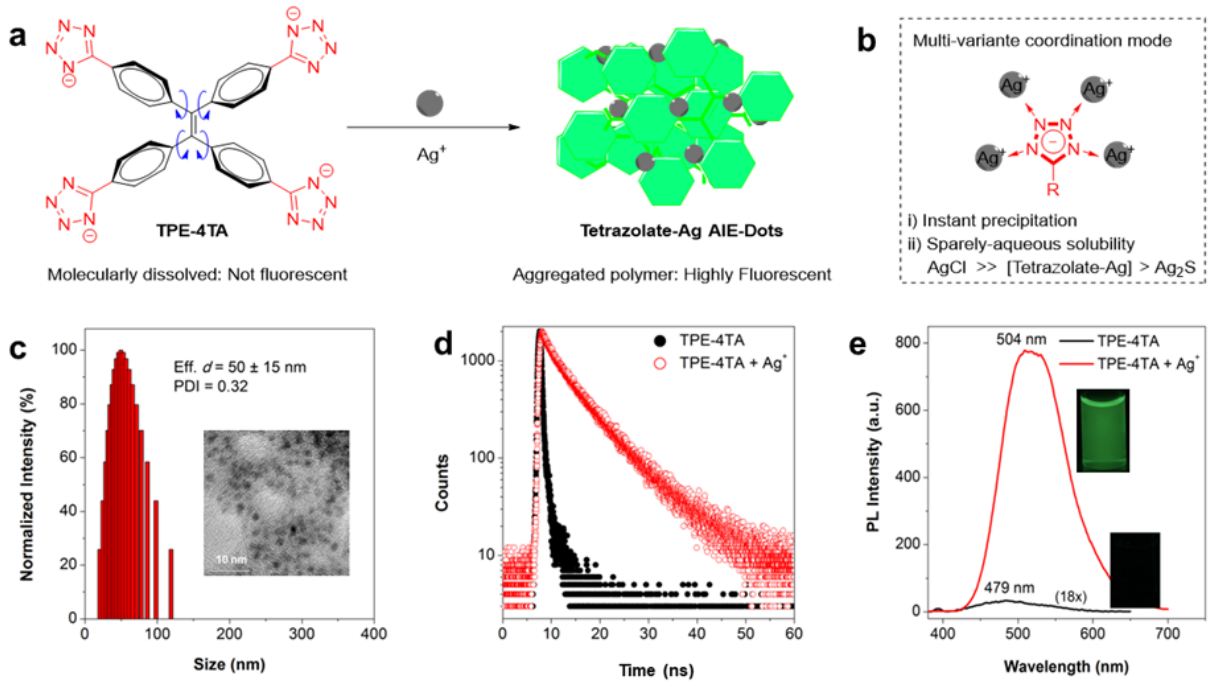

Figure 2. An Ag^+-triggered AIE process. (a) Schematic illustration of **TPE-4TA** turn-on by Ag^+ binding. (b) The multivariate coordination chemistry between the tetrazolate ion and silver ions. (c) The photoluminescence intensity of **TPE-4TA** alone or in the presence of Ag^+. (d) Fluorescence lifetime measurement of **TPE-4TA** alone or in the presence of Ag^+. (e) Characterization of the particle diameter of silver-AIE dots formed in the colloid solution by DLS. The image of these nanoparticles was analyzed by TEM and shown in the inset.

of **TPE-4TA** are therefore desirable to sense silver ions with high specificity and high-contrast fluorescence turn-on.

Optimization of histological staining by Ag+ and TPE-4TA

To assess the experimental condition required for **TPE-4TA** in sensing silver ions in histological stains for fluorescence *in situ* visualization, we first optimized silver impregnation from existing silver staining protocols that can specifically label nerve fibers, neurons, and fibrillary plaques. Histological staining methods such as the Golgi method, Gallyas silver stain, Bielschowsky's method, Peter's buffered silver staining method[33], Bodian's Method, and Cajal's double impregnation procedure are literally compared (supplementary table 1). These conventional stains varied dedicatedly from preparation of tissue slices, silver sources (acidic

silver or basic silver stains), buffering solvents (pH and salt concentrations), and incubation processes; but all stains generally use very high Ag^+ concentrations of 0.1–20% (*w*/*v*). When comparing the washing steps using water (supplementary Fig.1d–i) and 10% ethanol (supplementary Fig.1j–o) in initial attempts of silver-AIE staining, it was found that higher Ag^+ concentrations were required to give satisfactory results for stringent ethanol washes. Therefore, Ag^+ used in different embedding strategies needed to be titred respectively. Since the **TPE-4TA** probe has a detection limit in the nanomolar range for Ag^+, we subsequently scaled down the Ag^+ concentrations ten to two million folds in reference to the protocols using a silver concentration of 20% (*w*/*v*), whilst retaining the key steps in these silver-impregnation protocols.

After a serial titration of Ag^+ concentrations used in the silver-AIE stain, here we experimentally found that **TPE-4TA** in paraffin sections impregnated with 0.005% (*w*/*v*) Ag^+ or in 1-mm-thick intact cleared tissues impregnated with 0.00001% (*w*/*v*) Ag^+ exhibited good Signal to background ratio (SBR) and high fluorescence intensity for neurons, fibers, and myelinated structures. Furthermore, **TPE-4TA** staining of paraffin sections without silver impregnation showed only weak blue fluorescence in the background throughout the specimens, suggesting that Ag^+ is necessary for **TPE-4TA** to stain neural structures (supplementary Fig. 1a,b). The staining by **TPE-4TA** was not affected by autofluorescence as unstained paraffin-embedded tissue sections had minimal autofluorescence which did not interfere with image acquisition (supplementary Fig.1c). It was also shown that buffering the silver impregnation solution with 0.01 M borate-boric acid buffer to pH 8 reproducibly showed homogeneous fluorescence intensities with high brightness in the staining, and the addition of 0.0003% (*v*/*v*) of ammonium hydroxide (15 µl) in the second silver impregnation improved the contrast of the neurons and fibers from the background tissues (supplementary Fig. 2a). Under the optimized condition, the neuron-specific fluorescence signal in tissue sections was further confirmed to be dependent on tetrazole-silver complexes as **TPE-4TA** alone exhibited no specific staining at all (supplementary Fig. 2b).

Workflow of fluorogenic silver-AIE staining in hydrogel- or paraffin-embedded brain sections

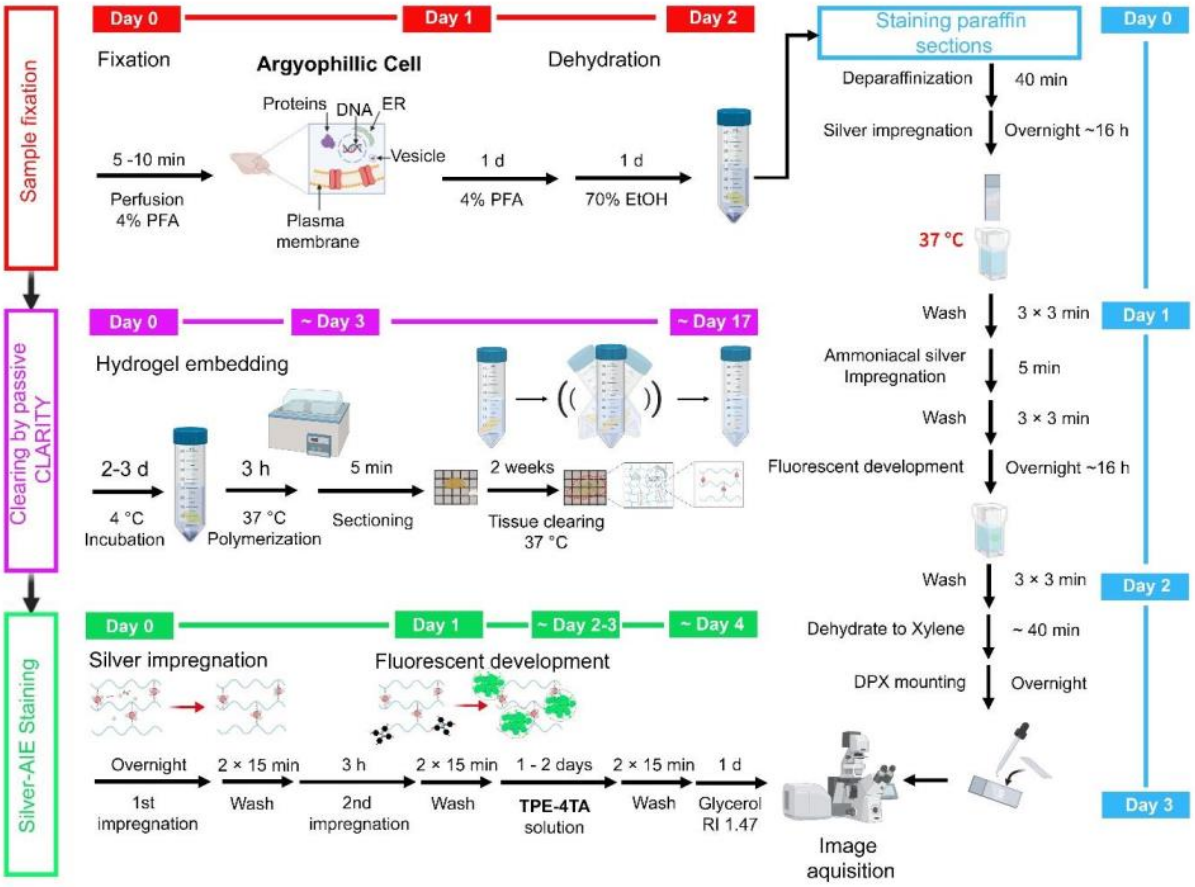

Figure 3. The fluorogenic silver-AIE staining pipeline. The fluorogenic silver method can be applied in fixed samples which can then be processed for paraffin 2D staining (in cyan color) or passive CLARITY clearing (in purple color) before being impregnated with silver nitrate and stained with the **TPE-4TA** dye.

After a systematic optimization, we established a protocol for the fluorogenic silver-AIE staining (Fig. 3). 8-µm-thick mouse brain slices post-fixed with 4% PFA were used as the model tissue sample and were stored in dry conditions at room temperature for subsequent embedding. Considering that brain slices have limited tissue opacity which hampers visualization of neural networks, we performed hydrogel embedding of whole mouse brain and clearing of 1 mm thick sections to reduce light scattering by extracting lipids from the tissues (Clearing by passive CLARITY). In comparison to unprocessed thick tissues specimens, hydrogel-embedded cleared tissues are optically transparent and gives better preservation of fluorescence which allow fluorescence imaging at greater penetration depths.[34–36]. Among different tissue clearing methods, passive Clear Lipid-exchanged Acrylamide-hybridized Rigid Imaging-compatible Tissue-hYdrogel (CLARITY) was chosen

in this study for the reason that it uses the same monomers of acrylamide and bis-acrylamide as the polyacrylamide gel which are compatible with **TPE-4TA** stain.[28,29] After tissue clearing with passive CLARITY, silver-AIE staining was carried out with double silver impregnation.

In the paraffin embedding approach, double silver impregnation was also adopted for the deparaffinized paraformaldehyde-fixed paraffin-embedded (PFPE). They were firstly incubated in a 0.005% $AgNO_3$ solution overnight followed by a few washes with ultrapure water. While staining without the use of ammonia resulted in a lower contrast for fine structures with more noticeable background staining, a second ammoniated silver impregnation with 0.0003% (*v*/*v*) of ammonium hydroxide (NH_4OH) for five minutes led to a more consistent stain and better delineation of neurons and fibers in cleared paraffin sections. Besides, silver concentrations and the incubation period in ammoniated silver are of paramount important variables to maintain staining specificity and consistency. For example, silver-AIE staining could be tuned to be myelin-specific to predominantly stain the white matter (supplementary Fig 2c). After a washing step to de-stain the non-specific bound silver ions, the tissue sections were incubated with the developing solution of 10 μM **TPE-4TA** for 16 hours. The samples were then fixed again after washing, dehydrated with ethanol in a graded series of concentrations, cleared with xylene, and mounted with dibutyl phthalate in xylene (DPX).

Comparison of silver-AIE stain with the Bielschowsky stain in brain slices

To evaluate the staining performance of the silver-AIE stain in PFPE sections, we compared it with the commercially available Bielschowsky's silver stain kit as a reference (Hito Bielschowsky OptimStain™ Kit, Hito corp.) which is optimized from the classic Cajal stain, the Bielschowsky silver method, and Peter's general silver stain. At low magnification, the Bielschowsky's silver stain kit stained the white matter in cerebellum and nerve bundles intensely, such as corpus callosum (CC) and anterior commissure (Figure 4a). In a side-by-side comparison of the Bielschowsky's silver staining and the fluorogenic silver-AIE staining in the coronal brain section, TPE-4TA generally gave more homogeneous staining in different regions, especially the cerebral cortex, caudate putamen, and hippocampus (Figure 4b). At high magnification, while the oversaturated or unsaturated signals of Bielschowsky's silver stain made it hard to distinguish individual neurons (Figure 4c–h), the silver-AIE method

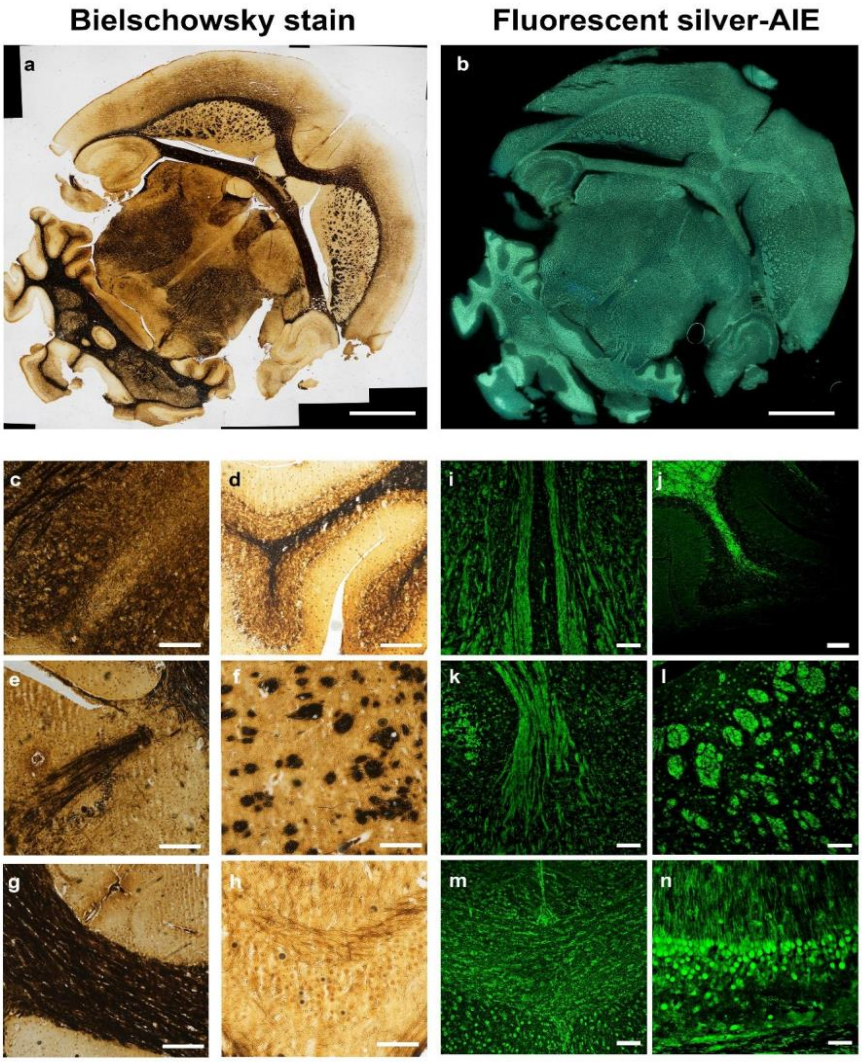

Figure 4. Comparison of staining in mouse brain sections by the Bielschowsky silver method and the AIE-silver method. (a) Stitched brightfield image of PFPE mouse brain sections stained by the Bielschowsky silver method. Bar: 1 mm. (b) Stitched widefield fluorescence image of PFPE mouse brain sections stained by the silver-AIE method. Bar: 1 mm. (c–h) Enlarged images of different brain regions in panel a. (i–n) Confocal images of the corresponding regions in panel c–h stained by the fluorogenic silver-AIE method**.** c and i: periaqueductal gray (PAG); d and j: cerebellum (cb); e and k: nerve fibers between PAG and cb; f and l: caudate putamen (CPu); g and m: corpus callosum (CC); h and n: hippocampus. Bars in c–g, i–m: 100 µm. Bars in h and n: 50 µm.

displayed comparable signal intensity for these neurons and nerve fibers in different brain regions (Figure 4i–n). Notably, the silver-AIE method gave exceptionally high SNR in the hippocampus that soma of individual neurons in the dentate gyrus (DG) and their projecting dendrites could be visualized clearly (Figure 4n).

Co-staining of silver-AIE stain with other nerve-specific stains

Next, we co-labeled the sample with other commonly used neuron-specific marker to evaluate the specificity and sensitivity of the silver-AIE stain. The neuronal nuclear protein (NeuN) is found in the nuclei and perinuclear cytoplasm of most neurons in the mammalian CNS.[39] Based on a published method that combines immunofluorescence and the Bielschowsky silver stain[40], simultaneous detection of neurons by NeuN immunofluorescence and silver-AIE was performed. Correlation of the signals from the silver-AIE stain and the NeuN labeling in transverse paraffin sections showed that their colocalization varied from area to area in the brain. In the dorsal lateral geniculate nucleus (DLG) of the thalamus, silver-AIE stain and NeuN labeled the same population of neurons with high Mander's correlation coefficient and Pearson correlation coefficient (Fig. 5a). In the caudate putamen (CPu), the silver-AIE stain also highlighted the myelinated fiber in addition to the soma, making it had less colocalization with NeuN (Fig. 5a). While in the area of superior semilunar lobule in the cerebellum (Crus1), silver-AIE predominantly stained the white matter tract and NeuN labelled the surrounding granule cells and some Purkinje cells (Figure 5a). Interestingly, Purkinje cells and granular cells could be stained by the silver-AIE method in the cleared cerebellum tissues (supplementary Fig. 6e) suggesting that the lipid-rich myelin sheaths may compete with neurons for silver ions during impregnation.

To further compare the staining pattern of NeuN and TPE-4TA, we prepared the paraffin sagittal sections to perform their co-staining. TPE-4TA stained the whole cerebellum robustly and NeuN stained mostly in the granular layer (supplementary Fig. 3a). In the regions of the splenium of the CC, NeuN only labeled the posterior cerebral cortex and subiculum, whereas TPE-4TA stained CC in addition to both regions (supplementary Fig. 3b). In the hippocampus, NeuN primarily labeled the cell bodies of the Pyramidal neurons in the stratum pyramidale, but TPE-4TA also stained the fibre of stria terminalis (supplementary Fig. 3c). It was also observed that TPE-4TA and NeuN labeled mostly the same but sometimes different subpopulation of neurons. In the DG and hippocampal CA2 region, some of the neurons were TPE-4TA-positive and NeuN-negative while some were TPE-4TA-negative and NeuN-positive (supplementary Fig. 3d–e). Besides DLG having the highest level of TPE-4TA and NeuN colocalization, other brain regions, such as

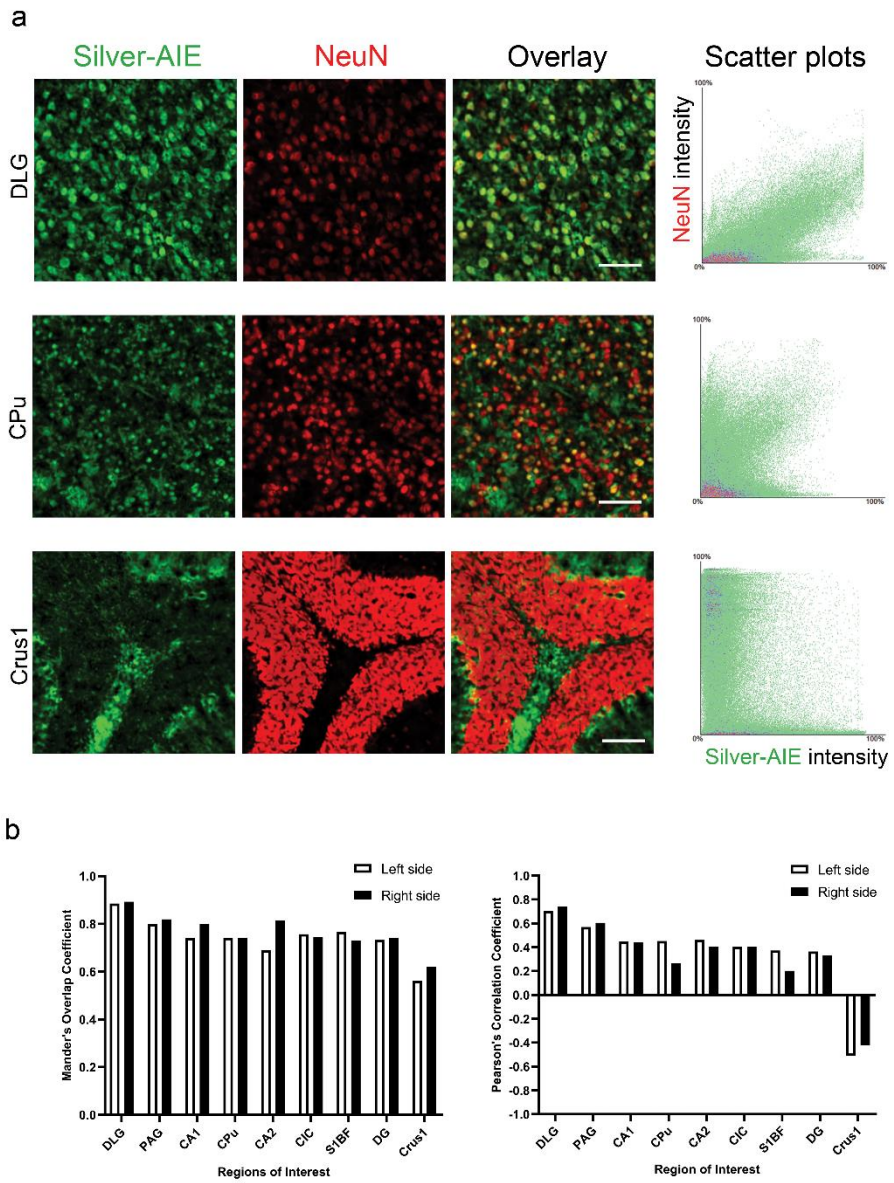

Figure 5. Simultaneous immunofluorescent and fluorescent silver-AIE co-staining. a, Fluorescent silver (Silver-AIE) and NeuN immunofluorescence co-stained regions of interests in the DLG (dorsal nucleus of lateral geniculate body), CPu (Caudate Putamen, Striatum) and Crus1 (Superior semilunar lobule, cerebellum) with their corresponding scatter plot. Images were denoised with NIS.ai and rolling ball background subtraction. Scale bar: 100 µm.

hippocampal CA2 and CA3, commissure of the inferior colliculus (CIC), CPu, periaqueductal grey (PAG), Crus 1, DG, and primary somatosensory cortex (S1BF), had varied staining pattern for TPE-4TA and NeuN (Figure 5b and supplementary Fig. 4). This implies that the argyrophilic property of neurons enables fluorescent visualization of both soma and nerve fibers by TPE-4TA, whereas immunolabeling of NeuN is restricted to the neuronal nuclei and soma where the antigen RBFOX3 is presence.

Use of silver-AIE stain in large-scale CLARITY cleared brain tissues and light sheet microscopy

Tissue clearing can render the tissue optically transparent by extracting lipids to reduce light scattering. This is particularly useful for the fluorescence 3D imaging analysis in large-scale samples to reveal the complex neural network. In the passive CLARITY method (Figure 3, highlighted in violet), the clearing step took about 17 days to turn half of the mouse brain into a highly transparent gel-like material (Figure 6a). In such condition, the tissue components including proteins and nucleic acids are largely fixed *in situ* by polymerization of acrylamide monomers.

We next evaluated the silver-AIE staining method in the cleared mouse brain. After silver impregnation, the CLARITY cleared mouse brain appeared to be pale-yellow which was primarily attributed to low levels of silver reduction from the glycerol mixture. Nonetheless, the whole specimen remained intact and highly transparency as illustrated by the normal morphological pattern of hippocampus (supplementary Fig. 5c–e). Under UV irradiation, the brain slice emitted strong fluorescence, but the fluorescence was more intensively localized on the edge of the sample (Fig. 6b). Since the pale-yellow color implied that the tissue sample is saturated with silver ions, we hypothesize that the Ag^+-**TPE-4TA** interaction in the outer regions may hinder the **TPE-4TA** molecules to penetrate into the inner part of the samples. To explore this possibility, we titrated the concentration of silver nitrate experimentally. It was found that 1% (*w*/*v*) silver nitrate in single impregnation led to high background fluorescence with no selective staining in neurons and the white matter (supplementary Fig. 6c), whereas 0.0001% (*w*/*v*) silver nitrate in the double impregnation are reduced quicker, so the silver ions in neuronal cells to prevent the tetrazole-silver ion complex from forming, resulting in no fluorescence within the cells (Supplementary Fig. 6a & b). By further reducing the amount of silver nitrate ten-fold to 0.00001% (*w*/*v*), the hippocampal neurons (Supplementary Fig. 6d), white matter tracts in the cerebellum (Supplementary Fig. 6e & 6f), CC (Supplementary Fig. 6g), and Purkinje cells (supplementary Fig. 6h & i) could be observed in 1mm thick cleared slices.

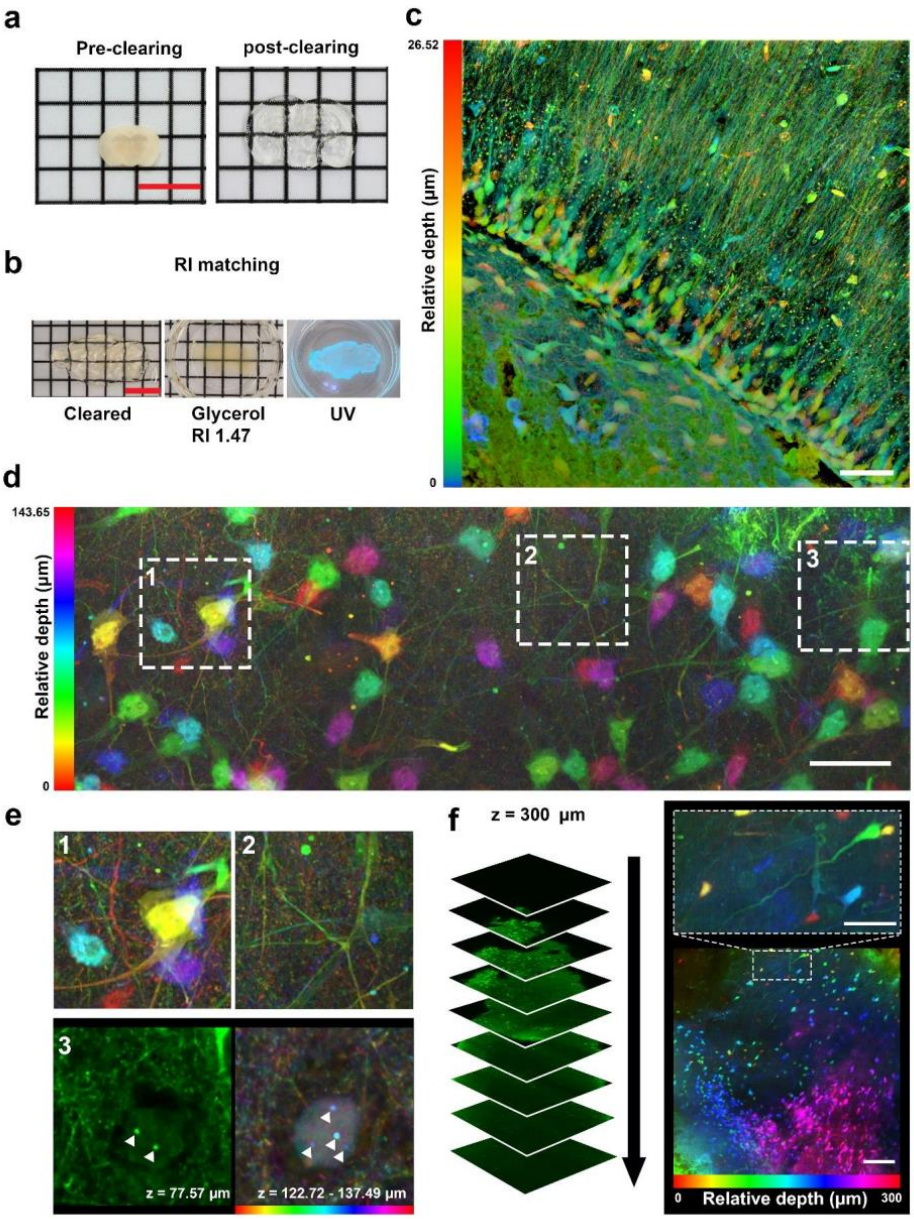

Figure 6. Fluorogenic silver-AIE staining in passive CLARITY cleared tissues. (a) Pre-clearing and post-clearing of a 1-mm thick coronal section of a mouse brain. Bar: 12 mm. (b) CLARITY cleared brain sections before (left) and after (middle) RI matching (1.47) with glycerol-water mixture and irradiated under UV (right). Bar: 12 mm. (c) Depth coded z-stack projection from 0 to 26.52 µm of a high dynamic range (HDR) confocal image in the hippocampus of a CLARITY cleared coronal section of a mouse brain. Bar: 50 µm (200 µm length × 200 µm width × 26.5 µm depth). (d) Depth coded z-stack projection of confocal images in the coronal section of the CLARITY-cleared cortical amygdala stained with the fluorogenic silver-AIE method. Scale bar: 50 µm (e) Corresponding enlarged region-of-interest in panel d denoised with Noise2void deep learning method showing a pyramidal neuron (1), a bipolar neuron (2), and Cajal bodies (3, arrowheads) at indicated z depths. (f) A tissue slab stained with the fluorogenic silver-AIE method were taken by light sheet microscopy in a z-stack of 300 µm and presented in a depth coded z-stack projection. Bar: 100 µm. Inset shows a zoom-in of a neuron. Scale bar: 30 µm.

In the depth-coded z-stack projection of confocal images with a thickness of 26.5 µm in

the hippocampal Cornu Ammonis region (CA), individual soma of pyramidal neurons in the pyramidal cell layer with their projecting dendritic trees in stratum radiatum could be resolved in pseudocolor (Fig. 6c, arrows). Interior to the pyramidal layer, interneurons in stratum oriens could also be identified (Fig. 6c, arrowheads). On the other hand, in a z-stack imaging of the 143-μm thick cortical amygdala (Fig. 6d), this stain specifically labelled different types of neurons with their intricate networks of neurites and distinguished morphology, such as pyramidal neurons (Fig. 6e, 1) and bipolar neurons (Fig. 6e, 2). Moreover, several puncta unmasked in the weakly stained neurons were observed in the soma at certain imaging depths (Fig. 6e, 3; arrowheads). These are assumed to be Cajal bodies which are argyrophilic. To further validate the applicability of using silver-AIE stain in high throughput 3-D imaging of thick brain slices, we used light sheet microscopy to perform fast volumetric imaging[41]. The whole imaging process for a volume of 300×300×300 μm^3 brain slice took approximately 10 minutes to complete with a good SNR (Fig. 6f). In a depth-coded image, a multipolar neuron with an axon of as long as >150 μm long could be observed, suggesting the potential of using fluorogenic silver stain in tracing neuronal connectivity.

Discussion

This work addresses a fundamental need for visualizing neural structures in the brain with a high SNR. The present silver-AIE method endows the conventional silver staining with new advantageous characteristics in bright Ag^+-induced fluorescence emission. Silver ions that bind to the functional groups of amino acids in denatured proteins can be fluorescently developed using the Ag^+-sensitive **TPE-4TA** probe. Given that it involves *in situ* self-assembly of metal-coordination polymers and an AIE-based fluorescence emission, the highly efficient signal amplification mechanism requires the Ag^+ concentration to trigger the fluorescence emission at least a thousand-fold lower than that used in the chromogenic silver staining protocols. Therefore, the fluorogenic silver-AIE method is much sensitive and has minimal background noise to reveal the biological structures that are not detectable by conventional chromogenic silver staining. This provides rich opportunities to apply the fluorogenic silver stain to systematic neuropathological analysis, such as visualization of dense-core plaques or cell density estimation in different brain regions.

In brain-mapping studies which rely heavily on a reference to register neurons or view the entire population of neurons, fluorogenic approach is advantageous in offering sufficient spatial resolution at cellular level. Immunofluorescence labelling and the silver-based fluorogenic stain are indispensable for histological studies of post-mortem brains, particularly in human brain samples where genetic, viral, and toxin tracers are not applicable. Despite the neuronal nuclear protein (NeuN), which is latterly identified as Rbfox3, is a neuronal marker widely used for the immunolabelling of most post-mitotic neuronal cells[42], it is in fact not ubiquitously expressed in all neuronal cell types[43]. In this regard, immunolabeling neurons with NeuN is not practical for Purkinje cells and olfactory mitral cells which do not express Rbfox3. The fluorogenic silver stain, on the other hand, visualizes neurons entirely at random. Notably, this fluorogenic silver method is widely compatible to other commonly used techniques in chemical fixation of mouse brain tissues and tissue staining methods such as immunofluorescence labelling. This allows the fluorogenic silver stain to be used as a complementary reference to other approaches.

In recent years, conventional silver staining methods have been modernized to suit for the advanced imaging platforms nowadays. Silver/gold-impregnated tissues can be imaged by laser scanning confocal microscopy through surface plasmon resonance with special optical filter sets to capture the shorter emission wavelengths in reference to the excitation wavelengths.[20] It can also be used in 3D electron microscopy with automated tracing algorithm to visualize ultrastructural details of Golgi-stained neurons.[21,22] In the present work, AIE mechanism of TPE-4TA enhances the sensitivity of silver development and overcomes the uncertainty of Ag^+ reduction in silver staining. We envision that this novel silver staining method provides a new staining strategy for brain tissues and can be applied to fluorescence imaging in unraveling architecture of brain connectivity.

Methods

Instruments

Fluorescence emission spectra were taken from a LS-55 fluorescence spectrophotometer (PerkinElmer). Transmission electron microscopy (TEM) images were obtained on a JEM 2010 transmission electron microscope. The fluorescence lifetime was measured using an

Edinburgh FLSP920 fluorescence spectrophotometer equipped with a xenon laser arc lamp (Xe900), a microsecond flash lamp (uF900), and a picosecond pulsed diode laser (EPL-375), and a closed cycle cryostat (CS202*I-DMX-1SS, Advanced Research Systems). Dynamic light scattering (DLS) experiments were conducted on a Malvern Zetasizer Nano ZS with a backscattering angle of 173°, using polystyrene latex (RI: 1.59, Abs: 0.010) as the parameters.

Tissue preparation

Animals

Male C57BL/6J mouse (2–3 months old) were obtained from The Hong Kong University of Science and Technology (Hong Kong, China) and were used for experiments. Animal experiments were approved by the Animal Ethics Committee and carried out in accordance with the institutional guidelines which conform to international guidelines.

Fixation of mice brain

C57BL/6J mice were anesthetized with diethyl ether and decapitated. The mouse brains were rapidly removed on ice, post-fixed in 4% PFA (Sigma-Aldrich), and stored in 70% ethanol at 4ºC prior to paraffin embedding or tissue clearing.

Paraffin section processing and staining

Embedding

Fixed C57BL/6J mouse brains were dehydrated sequentially in ethanol, xylene, and infiltrated with paraffin wax using a tissue processor (ThermoFisher, Excelsior™ AS Tissue Processor). Processed brains were then embedded in paraffin wax (Thermo Shandon Histocentre 3), sectioned to a thickness of 8 μm on a microtome (Leica, RM 2235S), and mounted onto slides.

Fluorogenic silver staining of paraffin-embedded sections

First, PFPE tissue sections were deparaffinized twice in xylene for 5 min each, twice in absolute ethanol, twice in 95% ethanol, twice in 75% ethanol, twice in 50% ethanol, and thrice

in ultra-pure water (18.0 Ω) for 3 min each. Then, each section was placed in 50 mL of 0.005% silver nitrate solution (Acros Organics) buffered with 0.01 M borate-boric acid buffer, pH 8.0 made from sodium tetraborate (J&K Scientific) and Boric acid (Sigma Aldrich). Silver impregnation was performed in a coplin jar for 16 h at 37ºC in the dark. Next, the tissue section was washed thrice in ultrapure water for 3 min each. Afterwards, 15 µl of 26–30% ammonium hydroxide (J&K Scientific) was added dropwise (5 µl each) to new silver solution for second silver impregnation which was performed for exactly 5 min. Finally, the tissue section was washed thrice in ultrapure water for 3 min each and placed in 50 mL of 10 µM **TPE-4TA** overnight in the dark for fluorescence development. After washing, the tissue section was dehydrated in ethanol and xylene before mounting. DPX mountant (Sigma-Aldrich) was used to mount a No. 1.5H glass coverslip (Paul Marienfeld).

CLARITY tissue clearing and staining

Hydrogel preparation

The hydrogel solution was prepared on ice by mixing 20 mL of 40% (*w*/*v*) acrylamide solution (Bio-Rad), 2.5 mL of 2% (*w*/*v*) bis-acrylamide solution (Bio-Rad), 20 mL of 10× phosphate buffered saline (PBS), pH 7.4 (Sigma-Aldrich), 0.5 g of 0.25% (*w*/*v*) VA-044 (J&K Scientific), and 157.5 mL of distilled water. The entire process was kept in dark where possible and stored at -20ºC for later use.

Thick coronal tissue sectioning

PFA-fixed or hydrogel-embedded whole mouse brains were sectioned into 1-mm coronal tissue slabs on a coronal mouse brain matrix with matrix blades (RWD Life Science) prior to tissue clearing.

Embedding and polymerization of hydrogel-tissue

1-mm Thick sectioned tissues or whole mouse brains were placed in a conical tube containing 50 mL of hydrogel solution for 3 or 7 d respectively at 4ºC. The conical tube was then placed in a desiccation chamber with the lid unscrewed for gas exchange. The chamber was purged with nitrogen gas, vacuumed, and finally purged again. The lid was immediately screwed back

on limiting exposure to atmospheric air and sealed with paraffin wax. The conical tube was then incubated in a water bath at 37ºC for 3 h to initiate polymerization of the hydrogel. Afterwards, excess hydrogel was removed gently by using Kimwipes®.

Passive tissue clearing

The clearing solution contained 0.2 M of boric acid and 80 g of SDS (4% wt/vol) with the final pH adjusted to 8.5 using 1 M NaOH. The sample was placed into a conical tube with 50 mL of clearing solution at 37–55ºC on a shaker for 3–14 days depending on the tissue size. Clearing solution was exchanged every 1–3 d. After clearing, the samples were washed with 0.1% Triton X-100 in 0.1 M borate-boric buffer, pH 8.5 twice a day at 37ºC, followed by an overnight wash in 0.01 M borate-boric buffer, pH 8.5, and a final change of buffer solution. The sample was stored in 4ºC until subsequent staining.

Fluorogenic silver-AIE staining of 3D cleared mouse brain tissue

The cleared tissue was impregnated with 50 mL of 0.005% silver solution buffered with 0.01 M borate-boric acid buffer, pH 8.0 in a glass jar at room temperature for 24 h in the dark on a shaker at 15 rpm. Then, the cleared tissue was washed in 30 mL of ultra-pure water for 30 min followed by a second silver impregnation for 3 h. Next, the cleared tissue was developed in 10 µM **TPE-4TA** buffered with 0.01 M borate-boric acid, pH 8.0 overnight. The stained sample was briefly rinsed in ultra-pure water followed by RI matching with glycerol (1.47) by immersion with a change of solution overnight and on the next day at least 1 h prior to imaging.

Bielschowsky silver stain

Hito Bielschowsky OptimStain™ Kit (Hitobiotec) was used according to the manufacturer's manual.

Fluorescence developing solution

The AIE fluorescence developing solution was prepared by dissolving 3 mg of **TPE-4TA** in 50 mL of ultra-pure water to make 1 mM of stock solution. 15 µl of 1 M NaOH was added dropwise (5 µl each time) to the stock solution and vortexed in between.

Immunofluorescence

Dual immunofluorescence labeling and silver-AIE staining were achieved by first permeabilizing and blocking the brain section with 0.025% Triton X-100 (Sigma-Aldrich), 3% bovine serum albumin (Sigma-Aldrich), and 0.3 M glycine (Sigma-Aldrich) for 1 h at room temperature. Then the section was incubated with the recombinant Alexa Fluor 647 conjugated anti-NeuN antibody (abcam; ab190565) at 4ºC overnight. After rinsing the slides with PBS, the stained sections was fixed with 4% PFA at room temperature for 1 h followed by washing thrice in ultrapure water for 5 min each (remove any residual PBS or PFA). The section was then proceeded to the silver-AIE staining of PFPE tissue section.

Imaging acquisition and processing

Laser scanning confocal microscopy

Cleared samples were placed in a 29 mm glass bottom dish with 20 mm micro-well #1.5 cover glass (Cellvis) and immersed with RI 1.47 glycerol-buffer (0.01 M borate-boric acid, pH 8.0) mixture with a glass coverslip placed on top. Fluorescence signals were collected with a Zeiss LSM 880 confocal microscope equipped with a Plan-Neofluar 20×/0.8 objective, Plan-Apochromat 63×/1.4 oil-immersion objective, Gallium arsenide phosphide (GaAsP) detectors , and driven by the Zeiss ZEN software version 2.1 SP1 (Carl Zeiss); or a Nikon A1 confocal microscope equipped with a 10× or 20× objective, with a hybrid-scanner (galvano/resonant) , and driven by the NIS-Elements Advanced Research software version (Nikon). Fluorescence signals recorded used: 405 nm laser excitation and a 500-530 nm emission filter for **TPE-4TA**; 633 nm laser excitation and a 665 nm emission filter for NeuN. Fluorescence images were acquired in grayscale and pseudo-colour.

Light-sheet fluorescence microscopy

The cleared tissue was cut with a scalpel and glued to the metal holder; the imaging chamber was filled with RI 1.47 glycerol-buffer (0.01 M borate-boric acid, pH 8.0) mixture. Light-sheet microscopy was performed using a Zeiss Lightsheet Z.1 Selective Plane Illumination Microscope equipped with an EC Plan-Neofluar 5×/0.16 objective and Two high-speed, highly sensitive sCMOS cameras (pco.edge 5.5). Data was acquired using Zen Black edition with the following specifications: 6.03 µm sheet thickness, 1 × zoom, 2.88 µm z-step size, two-sided sheet illumination, 30 ms camera exposure time. Fluorescence signals of TPE-4TA were recorded using 405 nm laser excitation, 550nm shortpass (SP) emission filter and 580 nm longpass LP emission filter.

Widefield microscopy

Widefield imaging was performed using a Nikon Eclipse Ci upright microscope equipped with a 4×, 10× and 20× objective, Nikon RGB camera, and excited with a white light LED (XT640-W, Lumen dynamics). The Bielschowsky silver stain was imaged in transmitted light path. **TPE-4TA** was imaged using an UV-2A filter cube (excitation: 330–380 nm; dichromic mirror: 400 nm; emission: LP 410 nm). Data as acquired using NIS-Elements Advanced Research version 5.30.01(Nikon).

Image processing

Images taken with the Nikon A1 confocal microscope were denoised with NIS.ai deep learning method with rolling ball background subtraction in NIS-Elements Advanced Research. Colour-coded maximum intensity projections were made in FIJI (1.53c) using the temporal-color code command. Fig. 6c was denoised with gaussian filter. Fig. 6e, f were processed by denoising with the Noise2void plugin on Fiji.

Colocalization analysis

The Mander's overlap coefficient (MOC) and the Pearson correlation coefficient (PCC) were calculated by NIS Elements advanced research. The Fluorescence intensity profile plots were measured by Fiji (Fiji is just ImageJ).

Data availability

The data that support the findings of this study are available from the corresponding authors upon reasonable request.

Acknowledgements

We would like to acknowledge SBS Core Laboratories in The Chinese University of Hong Kong for provision of equipment and technical support in tissue processing and sectioning of paraffin-embedded samples. We thank Dennis Tsim and Priscilla Ngai (Chinetek Scientific) for their technical support and providing the use of the Nikon Ti A1 confocal microscope.

Competing interests

The authors declare no competing financial interests. A US patent (62/707,532 2017.11.07 US) has been filed for the **TPE-4TA** probe.

Reference

1 Oh SW, Harris JA, Ng L, Winslow B, Cain N, Mihalas S *et al.* A mesoscale connectome of the mouse brain. *Nature* 2014; **508**: 207-+.

2 Lein ES, Hawrylycz MJ, Ao N, Ayres M, Bensinger A, Bernard A *et al.* Genome-wide atlas of gene expression in the adult mouse brain. *Nature* 2007; **445**: 168–176.

3 Wang X, Allen WE, Wright MA, Sylwestrak EL, Samusik N, Vesuna S *et al.* Three-dimensional intact-tissue sequencing of single-cell transcriptional states. *Science (80-)* 2018; **361**: eaat5691.

4 Motta A, Berning M, Boergens KM, Staffler B, Beining M, Loomba S *et al.* Dense connectomic reconstruction in layer 4 of the somatosensory cortex. *Science (80-)* 2019; **366**. doi:10.1126/science.aay3134.

5 Wang Q, Ding SL, Li Y, Royall J, Feng D, Lesnar P *et al.* The Allen Mouse Brain Common Coordinate Framework: A 3D Reference Atlas. *Cell* 2020; **181**: 936-953 e20.

6 Li A, Gong H, Zhang B, Wang Q, Yan C, Wu J *et al.* Micro-optical sectioning tomography to obtain a high-resolution atlas of the mouse brain. *Science (80-)* 2010; **330**: 1404–1408.

7 Ecker JR, Geschwind DH, Kriegstein AR, Ngai J, Osten P, Polioudakis D *et al.* The BRAIN Initiative Cell Census Consortium: Lessons Learned toward Generating a Comprehensive Brain Cell Atlas. *Neuron* 2017; **96**: 542–557.

8 Fornito A, Zalesky A, Breakspear M. The connectomics of brain disorders. *Nat Rev Neurosci* 2015; **16**: 159–172.

9 Chon U, Vanselow DJ, Cheng KC, Kim Y. Enhanced and unified anatomical labeling for a common mouse brain atlas. *Nat Commun* 2019; **10**: 5067.

10 Livet J, Weissman TA, Kang H, Draft RW, Lu J, Bennis RA *et al.* Transgenic strategies for combinatorial expression of fluorescent proteins in the nervous system. *Nature* 2007; **450**: 56–62.

11 Gao R, Asano SM, Upadhyayula S, Pisarev I, Milkie DE, Liu TL *et al.* Cortical column and whole-brain imaging with molecular contrast and nanoscale resolution. *Science (80-)* 2019; **363**. doi:10.1126/science.aau8302.

12 Eastwood BS, Hooks BM, Paletzki RF, O'Connor NJ, Glaser JR, Gerfen CR. Whole mouse brain reconstruction and registration to a reference atlas with standard histochemical processing of coronal sections. *J Comp Neurol* 2019; **527**: 2170–2178.

13 Daigle TL, Madisen L, Hage TA, Valley MT, Knoblich U, Larsen RS *et al.* A Suite of Transgenic Driver and Reporter Mouse Lines with Enhanced Brain-Cell-Type Targeting and Functionality. *Cell* 2018; **174**: 465-480 e22.

14 Kohl J, Ng J, Cachero S, Ciabatti E, Dolan MJ, Sutcliffe B *et al.* Ultrafast tissue staining with chemical tags. *Proc Natl Acad Sci U S A* 2014; **111**: E3805-14.

15 Fritzsch B, Muirhead KA, Feng F, Gray BD, Ohlsson-Wilhelm BM. Diffusion and imaging properties of three new lipophilic tracers, NeuroVue™ Maroon, NeuroVue™ Red and NeuroVue™ Green and their use for double and triple labeling of neuronal profile. *Brain Res Bull* 2005; **66**: 249–258.

16 Kang HW Moon BH, Lee SJ, Lee SJ, Rhyu IJ. KHK. Comprehensive Review of Golgi Staining Methods for Nervous Tissue. *Appl Microsc* 2017; **47**: 63–69.

17 Watson C, Kirkcaldie M, Paxinos G. Techniques for studying the brain. In: *The Brain*. Elsevier, 2010, pp 153–165.

18 Merchan MA de Castro F. DJ. *Cajal and de Castro's Neurohistological Methods*. Oxford University Press, 2016 doi:10.1093/med/9780190221591.001.0001.

19 Uchihara T. Silver diagnosis in neuropathology: Principles, practice and revised interpretation. *Acta Neuropathol* 2007; **113**: 483–499.

20 Thompson KJ, Harley CM, Barthel GM, Sanders MA, Mesce KA. Plasmon resonance and the imaging of metal-impregnated neurons with the laser scanning confocal microscope. *Elife* 2015; **4**. doi:10.7554/eLife.09388.

21 Kassem MS, Fok SYY, Smith KL, Kuligowski M, Balleine BW. A novel, modernized Golgi-Cox stain optimized for CLARITY cleared tissue. *J Neurosci Methods* 2018; **294**: 102–110.

22 Vints K, Vandael D, Baatsen P, Pavie B, Vernaillen F, Corthout N *et al.* Modernization of Golgi staining techniques for high-resolution, 3-dimensional imaging of individual neurons. *Sci Rep* 2019; **9**: 130.

23 Mei J, Leung NLC, Kwok RTK, Lam JWY, Tang BZ. Aggregation-Induced Emission: Together We Shine, United We Soar! *Chem Rev* 2015; **115**: 11718–11940.

24 Gao M, Tang BZ. Fluorescent Sensors Based on Aggregation-Induced Emission: Recent Advances and Perspectives. *ACS Sensors* 2017; **2**: 1382–1399.

25 Mei J, Huang Y, Tian H. Progress and Trends in AIE-Based Bioprobes: A Brief Overview. *ACS Appl Mater Interfaces* 2018; **10**: 12217–12261.

26 Chen S, Wang H, Hong Y, Tang BZ. Fabrication of fluorescent nanoparticles based on AIE luminogens (AIE dots) and their applications in bioimaging. *Mater Horizons* 2016; **3**: 283–293.

27 Xie S, Wong AYH, Chen S, Tang BZ. Fluorogenic Detection and Characterization of Proteins by Aggregation-Induced Emission Methods. Chem. - A Eur. J. 2019. doi:10.1002/chem.201805297.

28 Xie S, Wong AYH, Kwok RTK, Li Y, Su H, Lam JWY *et al.* Fluorogenic Ag+–Tetrazolate Aggregation Enables Efficient Fluorescent Biological Silver Staining. *Angew Chemie - Int Ed* 2018. doi:10.1002/anie.201801653.

29 Wong AYH, Xie S, Tang BZ, Chen S. Fluorescent Silver Staining of Proteins in Polyacrylamide Gels. *J Vis Exp* 2019. doi:10.3791/58669.

30 Carlucci L, Ciani G, Proserpio DM. Interpenetrated and Noninterpenetrated Three-Dimensional Networks in the Polymeric Species Ag(tta) and 2 Ag(tta)·AgNO3 (tta=tetrazolate): The First Examples of the μ4-η1:η1:η1:η1 Bonding Mode for Tetrazolate. *Angew Chemie Int Ed* 1999; **38**: 3488–3492.

31 Zhang J-P, Zhang Y-B, Lin J-B, Chen X-M. Metal Azolate Frameworks: From Crystal Engineering to Functional Materials. *Chem Rev* 2012; **112**: 1001–1033.

32 Lee JH, Kang S, Lee JY, Jung JH. A tetrazole-based metallogel induced with Ag+ ion and its silver nanoparticle in catalysis. *Soft Matter* 2012; **8**: 6557.

33 PETERS.A. A General-Purpose Method of Silver Staining By A. PETERS. *Sci Ind J* 1955; **96**: 323–328.

34 Chung K, Wallace J, Kim S-Y, Kalyanasundaram S, Andalman AS, Davidson TJ *et al.* Structural and molecular interrogation of intact biological systems. *Nature* 2013; **497**: 332–337.

35 Phillips J, Laude A, Lightowlers R, Morris CM, Turnbull DM, Lax NZ. Development of passive CLARITY and immunofluorescent labelling of multiple proteins in human cerebellum: understanding mechanisms of neurodegeneration in mitochondrial disease. *Sci Rep* 2016; **6**: 26013.

36 Jensen KHR, Berg RW. Advances and perspectives in tissue clearing using CLARITY. *J Chem Neuroanat* 2017; **86**: 19–34.

37 Brown M, Lowe DG. Recognising panoramas. *Proc IEEE Int Conf Comput Vis* 2003; **2**: 1218–1225.

38 Brown M, Lowe DG. Automatic Panoramic Image Stitching Automatic 2D Stitching. *Int J Comput Vis* 2007; **74**: 59--73.

39 Gusel'nikova V V, Korzhevskiy DE. NeuN As a Neuronal Nuclear Antigen and Neuron Differentiation Marker. *Acta Naturae* 2015; **7**: 42–47.

40 Segura-Anaya E, Flores-Miranda R, Martínez-Gómez A, Dent MAR. A novel histochemical method of simultaneous detection by a single- or double-immunofluorescence and Bielschowsky's silver staining in teased rat sciatic nerves. *J Neurosci Methods* 2018; **304**: 46–51.

41 Hillman EMC, Voleti V, Li WZ, Yu H. Light-Sheet Microscopy in Neuroscience. *Annu Rev Neurosci Vol 42* 2019; **42**: 295–313.

42 Kim KK, Adelstein RS, Kawamoto S. Identification of Neuronal Nuclei (NeuN) as Fox-3, a New Member of the Fox-1 Gene Family of Splicing Factors. *J Biol Chem* 2009; **284**: 31052–31061.

43 Mullen RJ, Buck CR, Smith AM. NeuN, a neuronal specific nuclear protein in vertebrates. *Development* 1992; **116**: 201–211.